



HAL
open science

Crustal structure of western Hispaniola (Haiti) from a teleseismic receiver function study

Jordane Corbeau, Frédérique Rolandone, Sylvie Leroy, K. Guerrier, D. Keir, G. Stuart, V. Clouard, R. Gallacher, S. Ulysse, D. Boisson, et al.

► **To cite this version:**

Jordane Corbeau, Frédérique Rolandone, Sylvie Leroy, K. Guerrier, D. Keir, et al.. Crustal structure of western Hispaniola (Haiti) from a teleseismic receiver function study. *Tectonophysics*, 2017, 709, pp.9-19. 10.1016/j.tecto.2017.04.029 . hal-01517419

HAL Id: hal-01517419

<https://hal.sorbonne-universite.fr/hal-01517419>

Submitted on 3 May 2017

HAL is a multi-disciplinary open access archive for the deposit and dissemination of scientific research documents, whether they are published or not. The documents may come from teaching and research institutions in France or abroad, or from public or private research centers.

L'archive ouverte pluridisciplinaire **HAL**, est destinée au dépôt et à la diffusion de documents scientifiques de niveau recherche, publiés ou non, émanant des établissements d'enseignement et de recherche français ou étrangers, des laboratoires publics ou privés.

Crustal structure of western Hispaniola (Haiti) from a teleseismic receiver function study

Corbeau J.^{1,2}, Rolandone F.¹, Leroy S.¹, Guerrier K.³, Keir D.^{4,5}, Stuart G.⁶, Clouard V.², Gallacher R.⁴, Ulysse S.³, Boisson D.³, Bien-aimé Momplaisir R.³, Saint Preux F.⁷, Prépetit C.⁷, Saurel J-M.², Mercier de Lépinay B.⁸ and Meyer B.¹

¹Sorbonne Universités, UPMC Univ Paris 06, CNRS, Institut des Sciences de la Terre de Paris (ISTeP), 4 place Jussieu, 75005 Paris, France

²Now at Observatoire Volcanologique et Sismologique de Martinique (OVSM), Institut de Physique du Globe de Paris (IPGP), UMR 7154, CNRS Sorbonne Paris Cité, Paris, France

³URGeo, Faculté des Sciences, Université d'Etat d'Haiti, Port-au-Prince, Haiti

⁴Ocean and Earth Science, National Oceanography Center Southampton, University of Southampton, Southampton, SO14 3ZH, UK

⁵Dipartimento di Scienze della Terra, Università degli Studi di Firenze, Florence 50121, Italy

⁶Institute of Geophysics and Tectonics, School of Earth and Environment, University of Leeds, Leeds, LS2 9JT, UK

⁷Bureau des Mines et de l'Énergie, Unité Technique de Sismologie, Port-au-Prince, Haiti

⁸Université Côte d'Azur, CNRS/IRD/OCA, Géoazur, Valbonne, France

Corresponding author: Jordane Corbeau, corbeau@ipgp.fr

1 **Abstract**

2 Haiti, located at the northern Caribbean plate boundary, records a geological history
3 of terrane accretion from Cretaceous island arc formations to the Eocene to Recent oblique
4 collision with the Bahamas platform. Little is presently known about the underlying crustal
5 structure of the island. We analyze P-waveforms arriving at 27 temporary broadband
6 seismic stations deployed over a distance of 200 km across the major terrane boundaries in
7 Haiti to determine the crustal structure of western Hispaniola. We compute teleseismic
8 receiver functions using the Extended-Time Multi-Taper method and determine crustal
9 thickness and bulk composition (V_p/V_s) using the H-k stacking method. Three distinctive and
10 fault-bounded crustal domains, defined by their characteristic Moho depth distributions and
11 bulk crustal V_p/V_s , are imaged across Haiti. We relate these domains to three crustal
12 terranes that have been accreted along the plate boundary during the northeastwards
13 displacement of the Caribbean plate and are presently being deformed in a localized fold
14 and thrust belt. In the northern domain, made up of volcanic arc facies, the crust has a
15 thickness of ~23 km and V_p/V_s of 1.75 +/- 0.1 typical of average continental crust. The
16 crust in the southern domain is part of the Caribbean Large Igneous Province (Caribbean
17 LIP), and is ~22 km thick with V_p/V_s of 1.80 +/- 0.03 consistent with plume-related rocks of
18 late Cretaceous age. Significantly thicker, the crust in central Haiti has values of Moho
19 depths averaging ~41 km and with V_p/V_s of 1.80 +/- 0.05. We propose that the central
20 domain is likely constructed of an island arc upper crust with fragments of dense material
21 originating from mafic lavas or LIP material. We produce a crustal profile along a N-S
22 transect across Haiti accounting for the surface geology, shallow structural history, and new
23 seismological constraints provided by variations of crustal thickness and bulk composition.

24

25

26 **Keywords:** Receivers Function, Haiti, crustal structure

27

28 **1- Introduction**

29 **1.1- Overview**

30 One of the keys to understanding the transpressive northern Caribbean plate
31 boundary and its geodynamic evolution is constraining crustal thickness and composition.
32 Several geological field studies have led to a description of the shallow structure and
33 stratigraphy of the island of Hispaniola (e.g., Mann et al., 1995; Pubellier et al., 2000). The
34 M_w 7.0 2010 Haiti earthquake prompted several geological and geophysical studies to
35 constrain the fault geometry and the crustal structure in the area of the mainshock (e.g.,
36 Douilly et al., 2013). However, our knowledge of the mid- and lower-crustal tectonics
37 remains very limited in the absence of whole crustal geophysical studies in Haiti. In
38 Dominican Republic, the eastern part of Hispaniola Island, interpretation of crustal
39 thickness from gravity data shows thick crust below the southern flank of the Dominican
40 Central Cordillera (Bowin, 1976). From April 2013 for nearly 14 months, a temporary
41 seismic network consisting of 27 stations was deployed in Haiti (Trans-Haiti project) to
42 determine its crustal thickness and bulk composition using teleseismic P-wave data. In
43 addition, we analyze seismograms from 3 permanent stations of the Canadian National
44 network (2010-2015) operated by the Bureau des Mines et de l'Energie and UTS. This paper
45 is the first one about works on temporary deployment of seismometers cross-cutting the
46 whole of the island.

47 The purpose of the present study is to determine crustal structure across Haiti from
48 receiver function (RF) analysis below Haiti so as to better constrain plate scale tectonic
49 evolution of the region responsible for the development of the current fold–thrust belt
50 (Mann et al., 1995; Pubellier et al., 2000; Hernaiz Huerta et al., 2007). The receiver
51 function analysis technique is an appropriate approach to image major discontinuities
52 within the crust and upper mantle from incoming teleseismic P-waveforms (e.g. Ammon,
53 1991).

54

55 **1.2- Geological and tectonic setting of Haiti**

56 Haiti, the western part of the Hispaniola island, is located on the Northern Caribbean
57 plate boundary, which separates the Caribbean plate from the North American plate (Fig.
58 1). Currently, the Caribbean plate moves in a east-northeast direction at about 20 mm/yr
59 relative to the North American plate (Symithe et al., 2015). As the plate boundary is
60 oriented E-W and the displacement vector of the Caribbean plate is about $N70^\circ$, the area
61 undergoes oblique collision and transpression at a large restraining bend in the strike–
62 slip plate boundary. The deformation of the Northern Caribbean plate boundary in Haiti is
63 partitioned and two major E-W left-lateral strike-slip faults, the Septentrional-Oriente
64 Fault Zone (SOFZ) in the North and the Enriquillo-Plantain-Garden Fault Zone (EPGFZ) in
65 the south with both faults accommodating the strike-slip component of the displacement
66 (Fig. 1). GPS geodesy shows that compression is mainly accommodated by Miocene to
67 recent folding and thrusting in the North–Haitian thrust fault and the Massif de la Selle
68 in southern Haiti (Symithe and Calais, 2016). The Trans-Haitian fold-and-thrust belt in
69 central Haiti (Fig. 1) was active until the late Neogene (Mann et al., 1995) but does not

70 appear to accommodate significant shortening today.

71 The geological and geodynamical history of Haiti is complex, however, two distinct
72 domains have been identified. Haiti is part of the Cretaceous volcanic island arc constituted
73 at the boundary of the Pacific realm (Pindell et al., 2006) called the Greater Antilles arc.
74 The Greater Antilles volcanic arc was initiated by an eastward dipping subduction in Central
75 America (Pindell et al., 2012; Van der Lelij, 2013; Hastie *et al.*, 2013). The Greater Antilles
76 arc now consists of a part of Cuba, Hispaniola and Puerto Rico islands (Mann et al., 1995).
77 This island arc constitutes two thirds of Hispaniola Island, and is mainly made up of arc
78 magmatic facies (Boisson, 1987; Escuder Viruete et al., 2006). The southern part of Haiti
79 has been interpreted to be part of the Caribbean Large Igneous Province (LIP), formed
80 during the Cretaceous on the Pacific Farallon plate, over the Galapagos hotspot (Duncan
81 and Hargraves, 1984). The LIP outcrops as a tholeiitic substratum associated with Upper
82 Cretaceous sediments in the Southern Peninsula of Haiti (Calmus, 1983), and has been
83 imaged south and west of Haiti with refraction and reflection data (Leroy et al., 2000;
84 Mauffret et al., 2001; Corbeau et al., 2016a). The volcanic island arc and the LIP
85 subsequently moved north- and eastwards from their Pacific position between the North
86 and South American plates, thus partitioning the current Caribbean plate (Pindell, 2012).
87 The Greater Antilles arc became an inactive intra-oceanic arc at the end of the Upper
88 Cretaceous when it collided with the Bahamas carbonate platform (Leroy et al., 2000; Cruz-
89 Orosa et al., 2012; Iturralde-Vinent et al., 2006). Between the island arc and the LIP lies
90 the Quaternary Cul-de-Sac sedimentary basin (Fig. 1), which is bounded to the North by the
91 thrusts of the Trans-Haitian belt, also called Haiti fold and thrust belt. This belt is formed
92 of NW-SE thrusts having propagated towards the SW since the Lower Miocene (Pubellier et

93 al., 2000).

94

95 **1.3- Previous geophysical work**

96 Previous geophysical studies have placed crude constraints on crustal structure in the
97 south and in the vicinity of Haiti that help place our results in context and aid
98 interpretation.

99 A compilation of seismic refraction data acquired in the Caribbean plate shows that
100 the thickness of the crust is not uniform (Diebold et al., 1981; Mauffret and Leroy, 1997;
101 Mauffret et al., 2001). The Caribbean oceanic crust is 5-km thick in Haitian sub-basin,
102 Colombia and Venezuela basins (Fig. 1). In the middle of the Caribbean plate, the original
103 oceanic crust is underplated by ultra-mafic material (Leroy et al., 2000), forming a LIP of
104 ~10 to 15 km in thickness. The Beata Ridge (Fig. 1), 20-30 km thick, is composed of oceanic
105 crust underplated by an ~15-20 km higher velocity (6 to 8 km/s) ultra-mafic magmatic
106 material and covered by a thin volcanic layer of ~2 km (basaltic with a P-wave velocity of
107 4.5 to 6 km/s). Submersible sampling along the Beata Ridge to the South of Haiti (Mauffret
108 et al., 2001) confirmed the deep origin of the underplated materials that are ultra-mafic
109 rocks such as picrites or komatiites (Revillon et al., 2000).

110 In addition, Douilly et al. (2013) provide a velocity model for the crust in the
111 southern part of Haiti, and show that the mean V_p/V_s in this area is 1.80, which is typical
112 for oceanic crust mafic rocks (Christensen, 1996). Velocity model and receiver functions
113 studies made by Moreno et al. (2002) and Gonzalez et al. (2012) show that the depth of the
114 Moho is approximately 20 km in the south of Cuba. In eastern Hispaniola, a seismic
115 refraction study shows that the Moho is at approximately 24 km depth, and reaches roughly

116 30 km deep in the central part of Hispaniola (Nuñez et al., 2015). The S- and Lg-wave study
117 of McNamara et al. (2012) implies that the Moho in the southwestern part of Hispaniola is
118 20.6 km depth.

119

120 **2- Data and Method**

121 **2.1- Data**

122 We use data from the 27 broadband stations of the temporary Trans-Haiti network
123 deployment (April 2013 - June 2014), spanning Haiti from North to South (Fig. 2). This
124 unique data set used SEIS-UK and iSTeP UPMC instruments that included 15 CMG-40TD and
125 12 CMG-6TD seismometers (30s natural period, 100 sps sampling rate). Additionally, we use
126 data from 3 broadband permanent stations of the Canadian National Seismic network
127 installed in Haiti after the 2010 Mw 7.0 earthquake and co-operated by the Bureau des
128 Mines et de l'Energie - UTS (Fig. 2).

129 To construct receiver functions we use seismograms from teleseismic earthquakes of
130 magnitudes $M_w > 5.0$, with epicentral distances between 30° and 90° . The initial data set
131 includes a total of 580 events recorded by the Trans-Haiti stations between April 2013 and
132 June 2014, and 2473 events for the Canadian stations between February 2010 and August
133 2015. The data are generally noisy, due to cultural noise sources, and a second order
134 Butterworth filter with corner frequencies of 0.03 and 2 Hz is applied to the data prior to
135 analysis. A visual quality control is subsequently performed on all the data such that only
136 seismograms that have clear direct-P arrivals are used to produce receiver functions. This
137 results in a reduced data set of 149 event records, with a range of between 2 and 13 per
138 station. A map showing the epicentral distribution of the analyzed earthquakes is given in

139 Fig. 3. Note that the majority of the events arrive from the south of the seismic network.

140

141 **2.2- Receiver function technique**

142 To image the crustal structure beneath Haiti we use the receiver function (RF)
143 method (e.g. Ammon, 1991), which is a deconvolution technique for isolating the P-to-S
144 converted phases (Ps) and associated reverberations (PpPs and PsPs + PpSs) of an incoming
145 P-waveform beneath a seismic station. The incident P-wave on the vertical component is
146 deconvolved from the radial and tangential components to remove source complexity and
147 leave a series of pulses that represent the P-to-S phase conversions (the so-called receiver
148 function).

149 Several deconvolution methods have been developed with different noise
150 stabilization processes: deconvolution in the frequency domain (Langston, 1979; Owens et
151 al., 1983; Ammon, 1991); deconvolution in the time domain by least squares estimation
152 (Abers et al., 1995); iterative deconvolution in the time domain (Gurrola et al., 1995;
153 Ligorria and Ammon, 1999) and multi-taper frequency domain cross-correlation (MTRF)
154 (Park and Levin, 2000; Helffrich, 2006). The advantage of the last method is that it works
155 on the correlated signal and mitigates against noise on the RFs. It has been recommended
156 in the case of oceanic island studies, such as the Cape Verde islands (Helffrich et al., 2010),
157 the Seychelles islands (Hammond et al., 2013), and the Canary islands (Lodge et al., 2012;
158 Martinez-Arevalo et al., 2013), and in our case we choose it for its capacity to remove
159 anthropic noise.

160 To estimate the Moho depth below the island of Haiti, we use the Extended-Time
161 Multitaper Frequency domain Cross-Correlation Receiver-Function (ETMTRF) technique of

162 Helffrich (2006), which is based on the MTRF method of Park and Levin (2000). The ETMTRF
 163 method uses a series of short and overlapping multiple tapers which window the time series
 164 across its full length, and sum the individual Fourier transformed signals to produce a RF
 165 estimate.

166

167 2.3- Moho depth and Vp/Vs estimation

168 We use a receiver function stacking technique (H- κ stacking) developed by Zhu and
 169 Kanamori (2000) to estimate the Moho depth (H) and the bulk crust ratio V_p/V_s (κ). This
 170 method uses the following equations (1), (2), (3), and (4) for stacking the RFs, and gives the
 171 results on a 10,000 point grid which shows the plausible range of values for H on increments
 172 of 0.4 km between 10 and 50 km and κ on increments of 0.004 between 1.6 and 2.0
 173 (Christensen, 1996):

$$174 \quad s(H, \kappa) = \sum_{j=1}^N w_1 r_j(t_1) + w_2 r_j(t_2) - w_3 r_j(t_3), \quad (1)$$

$$175 \quad t_1 = H \left[\sqrt{\frac{1}{V_s^2} - p^2} - \sqrt{\frac{1}{V_p^2} - p^2} \right], \quad (2)$$

$$176 \quad t_2 = H \left[\sqrt{\frac{1}{V_s^2} - p^2} + \sqrt{\frac{1}{V_p^2} - p^2} \right], \quad (3)$$

$$177 \quad t_3 = 2H \sqrt{\frac{1}{V_s^2} - p^2}, \quad (4)$$

178 where w_1 , w_2 , w_3 are weights, $r_j(t_i)$ are the amplitudes at the arrival times for each of
 179 the raypaths evaluated, N is the number of receiver functions, and p is the ray
 180 parameter determined from the IASPEI travel time tables (Kennet, 1991). The weights were

181 chosen as $w_1 = 0.5$, $w_2 = 0.3$ and $w_3 = 0.2$ as suggested by Zhu and Kanamori (2000). The
182 errors in the results were calculated by taking the maximum axes of the 95% confidence
183 interval of the grid plotted using the Zhu and Kanamori (2000) stacking method. The H- κ
184 stack was performed assuming a mean crustal P-wave velocity (V_p) of 6.6 km/s. This mean
185 crustal P-wave velocity comes from a study of the Pg seismic phase over Hispaniola
186 (McNamara et al., 2012). Crustal thickness, H, and average Vp/Vs determination is not very
187 sensitive to variations in the average Vp, as pointed out by Zhu and Kanamori (2000), and
188 testing Vp within the range 6.4-6.7 km/s on increments of 0.1 km/s provides very similar
189 results of H and Vp/Vs ratio.

190 Our final analysis uses the RFs computed from 149 earthquakes, from which one or
191 more reverberant Moho phases (PpPs or PpSs + PsPs) were clearly identifiable.

192

193 3- Results

194 Of the 30 stations, 27 yielded receiver functions with coherent P-to-S arrivals. Of
195 these, 19 displayed PpPs and PpSs + PsPs arrivals as well as Ps, enabling H- κ analysis (Table
196 1). Examples of stacked receiver functions and H- κ plots for stations PIGN, LGNH, and
197 MGOA are shown in Figure 4. For the 8 stations at which no clear reverberant phases were
198 found automatically by the program, RFs were combined to form single station stacks and
199 enhance the signal of the reverberations. At these stations, a clear Ps arrival is identifiable
200 and can be picked manually, but the H- κ stacking technique cannot be performed. We can
201 still however estimate the Moho depth using equation (2) and by assuming a Vp/Vs ratio
202 after several tests. Final Vp/Vs ratios chosen are the values providing arrival times for the
203 PpPs and PpSS + PsPs reverberations that match the signal stacks, and which are coherent

204 with the V_p/V_s of the surrounding stations (Table 2).

205 The results show large but systematic variations in Moho depth and V_p/V_s ratio
206 throughout Haiti (Figures 5 and 6). The Moho depths can be split into three main groups
207 shown in Fig. 5 and based on location and values (in latitudinal order GGIL, MEND, STRA,
208 PIGN and CAYH in the northern part of Haiti; BOIS, DROU, GADC, THOM, CANG, DUFF, MIRB,
209 ARCH, GIMB, BMCA, CBOQ, BMES, PAPH and LGNH in the central part, and MGOA, PETG,
210 GRBO, JAKH, JACM, FERM, FURC, and MARG in the southern part of Haiti).

211

212 3.1- Moho depths in Haiti

213 Results from the H-K stacking method in the northern domain of Haiti are well
214 resolved, with the stations STRA, PIGN and CAYH particularly well constrained. Results are
215 also consistent across this domain giving Moho depths of between 20.1 km and 28.2 km
216 (Table 1, Fig. 5).

217 Results in the southern part of Haiti are also well resolved, with the stations MGOA,
218 JACM and PETG particularly well constrained. Results across the domain give Moho depths
219 ranging between 16.1 km and 29.8 km, increasing in the center of the area at the stations
220 GRBO, MARG, FURC (Table 1, Fig. 5). The stations MARG and JAKH have clearly identifiable
221 Ps arrivals, but due to the lack of observable multiples the H-K stacking technique cannot
222 be performed. However, we can still estimate the depth of the Moho by using equation (2)
223 (Table 2, Fig. 5).

224 Our results show that the central part of Haiti exhibits greater Moho depths than in
225 the northern and southern parts, with a Moho discontinuity always deeper than 30 km. The
226 RFs of the stations located in this part of Haiti are more complicated due to intracrustal

227 reverberations, probably due to sediments layers. However, consistent values are found for
228 the stations THOM, CANG, DUFF, BMCA, CBOQ, DROU, LGNH and BOIS with Moho depths
229 ranging between 34.6 km and 45.2 km (Table 1, Fig. 5). We estimate the Moho depth for
230 the stations GADC, MIRB, GIMB, BMES, ARCH, and PAPH by assuming a V_p/V_s ratio from the
231 closest stations (Table 2, Fig. 5). Transect A in Fig. 7 shows the abrupt change in Moho
232 depth of ~10 km between the southern part and the central part of Haiti.

233

234 **3.2- V_p/V_s ratio**

235 The average crustal V_p/V_s ratio is sensitive to the bulk composition of the crust
236 (Zandt and Ammon, 1995; Chevrot and Van der Hilst, 2000, Stuart et al., 2006). Mineralogy
237 is an important factor influencing V_p/V_s ratio (Christensen, 1996): For felsic quartz-rich
238 rocks, such as granite, V_p/V_s ratio is ~1.71; for intermediate rocks, such as diorite, V_p/V_s
239 ratio is typically ~1.78; and for mafic rocks, such as gabbro V_p/V_s ratio is ~1.87. Higher
240 values of V_p/V_s ratio are associated with the presence of partial melting or fluids
241 (Watanabe, 1993; Thompson et al., 2010).

242 The V_p/V_s ratio over Haiti ranges from 1.64 to 1.99 (Fig. 6) suggesting a wide range
243 of mineral composition lateral variation. In particular, the stations MEND, CANG, BMCA and
244 LGNH show particularly high V_p/V_s ratios of 1.94, 1.99, 1.98 and 1.96 respectively (Fig. 6).
245 We observe that these stations are located on or near major tectonic features (Fig. 2), and
246 therefore fluid migration along active faults could feasibly locally increase the V_p/V_s ratio.
247 In order to interpret regional variations in crustal structure and since the interstation
248 variability is relatively high, we calculate the mean V_p/V_s ratio for each of the 3 domains
249 identified in Fig. 5, excluding the four very high values. Regional averages of V_p/V_s seem to

250 provide more insights than single-station values, excepting for particularly high values that
251 could show fluid migration (Rossi et al., 2006). The mean V_p/V_s ratio is 1.75 ± 0.10 in the
252 northern part of Haiti, 1.80 ± 0.05 in the central part, and 1.80 ± 0.03 in the southern part.

253

254 **3.3- Shallow discontinuity**

255 In addition to P to S Moho converted phases, one station, CAYH, exhibits another
256 clear shallow discontinuity. The RF plot for station CAYH versus back-azimuth (top of Fig. 8)
257 shows a shallow discontinuity in the first 2 s of the signal, prior to the P_s arrival from the
258 Moho. Clear Moho P_s arrivals are obvious just after 2 s, and are easily identified in the
259 upper RFs (group a, Fig. 8), coming from the south (back-azimuths between 176° and 178° ,
260 Fig. 8). The H-K stack method for this group gives a Moho depth of 22.1 km, which is
261 consistent with the closest station PIGN (Fig. 5 and Table 1), and a V_p/V_s ratio of 1.64. We
262 estimate the depth of the shallow discontinuity easily visible in the RFs of the group b
263 assuming that the upper crust has an average V_p of 5.8 km/s and an average V_p/V_s ratio of
264 1.77. These average properties are derived from the P velocity model in Haiti of Douilly et
265 al. (2013). This discontinuity is thus estimated at ~ 9.7 km depth.

266

267 **4- Discussion**

268 **4.1- Identification of 3 distinct crustal domains**

269 The depth distribution of the Moho in Haiti shows 3 distinct regions that we relate to
270 3 distinct geological domains (Fig. 9).

271 The Southern Peninsula of Hispaniola (Fig. 9) is known to be a part of the Caribbean
272 LIP, and to be composed of Cretaceous tholeiitic material (Calmus, 1983; Bien-Aimé

273 Momplaisir, 1986). In this part of the island, the Moho depths from our study vary from 16.1
274 km to 29.8 km along a W-E profile (Fig. 7E) and from 20.5 km to 27.5 km along a N-S profile
275 (Fig. 7A), giving an average crustal thickness of 22 ± 5 km. The variability of the Moho
276 depths we image in the Southern Peninsula may reflect the large differences in the LIP
277 thickness identified in previous studies between the oceanic crust and the areas with more
278 or less of underplated material (Diebold et al., 1981; Mauffret and Leroy, 1997; Leroy et
279 al., 2000; Mauffret et al., 2001). In our results the mean V_p/V_s ratio is 1.80 ± 0.03 ,
280 consistent with previous studies (Douilly et al., 2013) and the geology of the Southern
281 Peninsula (Calmus, 1983; Bien-Aimé Momplaisir, 1986). The northern limit of the LIP crustal
282 domain is given by the Moho depth calculated at the station LGNH (34.6 km; Fig. 5) and
283 could correspond to the trace of the EPGFZ (Fig. 2) in this area (south of LGNH), as
284 suggested by previous studies (Saint-Fleur et al., 2015).

285 The northern part of Hispaniola (Fig 9) is known to be a part of the Great Arc of the
286 Caribbean (Burke, 1988), an inactive intra-oceanic island arc formed in the Cretaceous at
287 the boundary of the Pacific domain and the proto-Caribbean oceanic crust (Pindell et al.,
288 2006). The Moho depth values we compute are ranging between 20.1 km and 28.2 km,
289 providing an average crustal thickness of 23 ± 3 km in agreement with the values found in
290 southern Cuba (approximately 20 km, Moreno et al., 2002; Gonzalez et al., 2012) and
291 eastern Hispaniola (about 24 km, Nuñez et al., 2015). Furthermore, our results delineate
292 the southwestern limit of the island arc domain. The shift of the Moho depths, from 22.1
293 km (CAYH) to 36.4 km (GADC), occurs across the trace of a major thrust evidenced by
294 geological studies (Figs 5 and 9). Both this major thrust and the sharp offset of the Moho
295 depths outline a distinct crustal domain to the west and south of this feature.

296 In addition to the southern and northern domains discussed above, we identify a
297 central domain distinct from both the LIP in the South and the island arc in the North (Fig.
298 9), which is characterized by a thicker crust ranging from 32.3 km to 45.4 km, with an
299 average of 41 ± 4 km. The relatively deep Moho is well constrained by 13 stations. In
300 addition, the preliminary results of a recent seismic refraction study by Nuñez et al. (2015)
301 indicate that the thickness of the crust increases from eastern Hispaniola towards the west
302 reaching a value of ~40 km at the boundary between Haiti and the Dominican Republic near
303 our profile. The Cul-de-Sac sedimentary basin (Fig. 1) and the Trans-Haitian belt belong to
304 the same thick domain, where the nature of the crust below these superficial structures has
305 still to be determined. We further discuss the different hypothesis regarding the nature of
306 the crust of this domain.

307

308 **4.2 Vp/Vs ratio**

309 We find very high Vp/Vs ratios, between 1.94 and 1.99 at four stations, located near
310 major faults: LGNH near the strike-slip EPGFZ and MEND, CANG and BMCA near the main
311 thrust faults (Figs. 2 and 6). High Vp/Vs ratios are often associated with partial melt,
312 basaltic intrusions or the presence of fluids (Stuart et al, 2006; Hammond et al., 2011). We
313 favor an explanation whereby the high Vp/Vs ratios associated with major crustal faults are
314 related to the presence of fluids within the fault zones (Thurber et al., 2003; Zhao et al.,
315 1996). Nevertheless, all the stations located near major faults do not present high Vp/Vs
316 values (e.g. CAYH, fig. 2).

317 The mean Vp/Vs ratio (1.80 ± 0.03) found in the southern domain is in agreement
318 with its late Cretaceous oceanic plateau origin (Christensen, 1996; Douilly et al., 2013). In

319 the northern domain composed of a late Cretaceous–Eocene, intra–oceanic volcanic arc
320 and forearc–accretionary prism, the V_p/V_s ratio of 1.75 ± 0.10 is close to that expected
321 for the average continental crust, 1.768 (Christensen, 1996). The central part of Haiti is
322 characterized by V_p/V_s ratio of 1.80 ± 0.05 , indicating that mafic rocks may be part of the
323 crustal lithology of this domain as in the southern domain.

324

325 **4.3- Implications for the tectonic history of Hispaniola**

326 We identify three distinct tectonic domains with different crustal thickness and bulk
327 composition. Based on our computed Moho depths and V_p/V_s ratios, and with additional
328 constraints from the major thrusts identified at the surface and the geodynamic
329 reconstructions (Leroy et al., 2000; Pubellier et al., 2000; Calais et al., 2016), we propose a
330 geological model along a N-S profile across Haiti (Fig. 10). This transect shows the LIP in the
331 South, the Cretaceous volcanic arc in the North, and a central thicker domain.

332 The central domain is characterized by relatively thick crust of ~41 km, between two
333 domains with significantly thinner crusts of 20-30 km. Surprisingly, the thick crust of the
334 central domain is not associated with major relief (~1 km). Based on field studies and
335 geodynamic reconstructions proposed for this area (e.g. Stéphan et al., 1990; Meschede and
336 Frisch, 1998; Mann et al 1991; Calais et al., 2016), the nature of the crust of the central
337 domain is likely to be island arc and fore-arc type, considered as either back-arc (Mann and
338 Lawrence, 1991) or a Cretaceous-Eocene remnant arc (Heubeck et al., 1991). Other
339 stratigraphic and tectonic studies (e.g. Pubellier et al., 2000) suggest that the fold-and-
340 thrust belt of this crustal domain may be rooted on the continuation of the rifted crust of
341 the eastern Cayman continental passive margin (Fig. 9). However, V_p/V_s ratio of 1.80,

342 typical for mafic rocks (average of values for this domain; Tables 1 & 2), may indicate that
343 the central crustal domain could not be composed only of island arc crust, and may imply
344 the presence of dense material. This dense material could be either related to Pliocene-
345 Quaternary mafic center of volcanism coming from an ancient continental mantle
346 lithosphere fragment (Kamenov et al., 2011) or associated to LIP material fragment coming
347 from the south and both trapped early in central Haiti. Geochemical studies of the LIP
348 south of Hispaniola from submersible dive samples (Revillon et al., 2000; Mauffret et al.,
349 2001) show indeed that the lower part of the LIP is made of ultra-mafic rocks and
350 geophysical studies (Mauffret and Leroy, 1997; 1999) evidence a high velocity layer
351 composed of dense material (velocity 7.5 to 7.9 km/s; density of 3 to 3.1; Herzberg et al.,
352 1983). The mafic Quaternary rocks are also MgO-rich (Kamenov et al 2011) and give high
353 V_p/V_s ratio.

354 On the transect in Fig. 10 we also draw the intracrustal discontinuity determined
355 from our receiver functions at the station CAYH. The estimated depth of this intracrustal
356 discontinuity (~10 km) may provide information on the possible depth for the Late-
357 Cretaceous to Pleistocene flysch of the Peralta belt (Witschard and Dolan, 1990; Dolan et
358 al., 1991), which outcrops at the front of the Cretaceous volcanic arc (Fig. 10). At the
359 surface, three major thrusts are geologically mapped (the Montagnes Noires, the Chaîne des
360 Matheux and the Gonâve Island; Fig. 1 and 2; Mann et al., 1995; Pubellier et al., 2000;
361 Hernaiz Huerta et al., 2007). In our transect, we propose to extend these thrusts to greater
362 depth along three large crustal slices (Fig. 10). The three major thrusts of the Trans-Haitian
363 belt show small cumulative throws at outcrop and little evidence of strong compressional
364 tectonics (Mann et al 1995; Pubellier et al 2000, Corbeau et al., 2016b). SW-vergent fold

365 and thrust belt related to the Hispaniola restraining bend and back arc basin collapse
366 (Heubeck et al., 1991) could have contributed to the overall thickening.

367

368 **5- Conclusions**

369 A receiver function study of 23 stations is used to determine the crustal structure
370 across Haiti, in order to place better constraints on the history and geometry of late
371 Cretaceous to recent terrane accretion. In the northern part of Haiti, consisting of the
372 Cretaceous volcanic island arc and forearc of the Greater Antilles, the Moho discontinuity is
373 imaged at a depth of ~23 km with Vp/Vs ratio of 1.75. In the southern part of Haiti, made
374 of the folded and thrustured Cretaceous oceanic Large Igneous Province (LIP), the Moho
375 depth is imaged at ~22 km, and Vp/Vs ratio is 1.80. In the central part of Haiti,
376 encompassing the Haitian fold-and-thrust belt, the Moho discontinuity is deeper with a
377 mean depth of ~41 km. We propose that this unexpected thick central domain with Vp/Vs
378 ratio of 1.80 corresponds to a distinct crustal domain. This domain is likely to consist of
379 island-arc type crust related to the Great Arc of the Caribbean, or the proximal part of the
380 Cayman Trough eastern passive margin, associated with mafic material coming from
381 fragments of lithospheric mantle from the north or mafic LIP material from the south.

382

383

384

385

386 **Acknowledgements**

387 The seismological equipment was loaned from the SEIS-UK equipment pool and from the
388 ITeP facilities. The facilities of SEIS-UK are supported by the Natural Environment

389 Research Council (NERC) under Agreement R8/H10/64. DK time on the research is funded
390 by NERC grant NE/L013932/1. This work could not have been done without Gérard Laborde
391 and DIGICEL, and without our collaboration with the Bureau des Mines et de l'Energie and
392 the Université d'Etat d'Haiti in Haiti. The paper benefits from fruitful discussions with
393 Nicolas Bellahsen and Claudio Rosenberg. We thank the Editor, the reviewer David
394 Schlaphorst and an anonymous reviewer for their constructive comments that helped
395 improved the manuscript.

396 **References**

- 397 Abers, G. A., X. Hu and L. R. Sykes, 1995. Source scaling of earthquakes in the Shumagin
398 region, Alaska : time-domain inversions of regional waveforms. *Geophysical Journal*
399 *International*, vol. 123, no 1, p. 41-58.
- 400
- 401 Ammon, C. J., 1991. The isolation of receiver effects from teleseismic P waveforms. *Bull.*
402 *Seismol. Soc. Am*, vol. 81, no 6, p. 2504-2510.
- 403
- 404 Bien-Aimé Momplaisir, R., 1986. Contribution à l'étude géologique de la partie orientale du
405 Massif de la Hotte (Presqu'île du Sud d'Haïti) : Synthèse structurale des marges de la
406 presqu'île à partir de données sismiques, thèse de doctorat, Ph. D. thesis, 210 pp., Univ.
407 Pierre-et-Marie-Curie (Paris VI), Paris.
- 408
- 409 Boisson, D., 1987. Etude geologique du massif du nord d'Haïti (Hispaniola-grandes Antilles),
410 thèse de doctorat, Ph. D. thesis, Univ. Pierre et Marie Curie (Paris VI), Paris.
- 411
- 412 Bowin, C.O, 1976. Caribbean Gravity Field and Plate Tectonics, Geological Society of
413 America Special Paper, vol. 169.
- 414
- 415 Burke, K.,1988. Tectonic evolution of the Caribbean, Annual Review of Earth and Planetary
416 Sciences, vol. 16, p. 201-230.
- 417
- 418 Calais, E. and B. Mercier de Lépinay, 1991. From transtension to transpression along the
419 northern Caribbean plate boundary off Cuba : Implications for the recent motion of the
420 Caribbean plate, *Tectonophysics*, vol. 186, no 3, p. 329-350.
- 421
- 422 Calais, E., S. Smithe, B. Mercier de Lépinay and C. Prépetit, 2016. Plate boundary
423 segmentation in the northeastern Caribbean from geodetic measurements and Neogene
424 geological observations, *Comptes Rendus Geoscience*, 348(1), 42-51.
- 425
- 426 Calmus, T., 1983. Contribution à l'étude géologique du massif de Macaya(sud-ouest d'Haïti,
427 Grandes Antilles) : sa place dans l'évolution de l'orogène Nord-Caraïbe, thèse de doctorat,
428 Univ. Paris VI, Paris.
- 429
- 430 Chevrot, S. and R. D. van der Hilst, 2000. The poisson ratio of the australian crust :
431 geological and geophysical implications, *Earth and Planetary Science Letters*, vol. 183, no
432 1, p. 121-132.
- 433
- 434 Christensen, N. I., 1996. Poisson's ratio and crustal seismology, *Journal of Geophysical*
435 *Research: Solid Earth* (1978-2012), vol. 101, no B2, p. 3139-3156.
- 436
- 437 Corbeau, J., F. Rolandone, S. Leroy, B. Mercier de Lépinay, B. Meyer, N. Ellouz-
438 Zimmermann and R. Momplaisir, 2016a. The Northern Caribbean plate boundary in the
439 Jamaica Passage: structure and seismic stratigraphy, *Tectonophysics*,
440 doi:10.1016/j.tecto.2016.03.022.

441 Corbeau, J., F. Rolandone, S. Leroy, B. Meyer, B. Mercier de Lépinay, N. Ellouz-
442 Zimmermann and R. Momplaisir, 2016b. How transpressive is the Northern Caribbean plate
443 boundary ?, *Tectonics*, doi:10.1002/2015TC003996.
444

445 Cruz-Orosa, I., F. Sàbat, E. Ramos, L. Rivero and Y. M. Vázquez-Taset, 2012. Structural
446 evolution of the La Trocha fault zone : Oblique collision and strike-slip basins in the Cuban
447 Orogen, *Tectonics*, vol. 31, no 5.
448

449 Diebold, J., P. Stoffa, P. Buhl and M. Truchan, 1981. Venezuela Basin crustal structure,
450 *Journal of Geophysical Research : Solid Earth (1978-2012)*, vol. 86, no B9, p. 7901-7923.
451

452 Dolan, J., P. Mann, R. de Zoeten, C. Heubeck, J. Shiroma and S. Monechi, 1991.
453 Sedimentologic, stratigraphic, and tectonic synthesis of Eocene-Miocene sedimentary
454 basins, Hispaniola and Puerto Rico, *Geological Society of America Special Papers*, vol. 262,
455 p.217-264.
456

457 Douilly, R., J. S. Haase, W. L. Ellsworth, M.-P. Bouin, E. Calais, S. J. Smithe, J. G.
458 Armbruster, B. Mercier de Lépinay, A. Deschamps, S.-L. Mildor and collab., 2013. Crustal
459 Structure and Fault Geometry of the 2010 Haiti Earthquake from Temporary Seismometer
460 Deployments, *Bulletin of the Seismological Society of America*, vol. 103, no 4, p. 2305-
461 2325.
462

463 Duncan, R. and R. Hargraves, 1984. Plate tectonic evolution of the Caribbean region in the
464 mantle reference frame, *Geological Society of America Memoirs*, vol. 162, p. 81-94.
465

466 Escuder Viruete, J., Contreras F., Stein, G., Urien, P., Joubert, M., Ullrich, T.D.,
467 Mortensen, J., Perez Estaun, A., 2006. Transpression and strike-slip partitioning in the
468 Caribbean island arc: fabric development, kinematics and Ar-Ar ages of syntectonic
469 emplacement of the Loma de Cabrera batholith, Dominican Republic, *Journal of Structural
470 Geology*, 28, 1496-1519.
471

472 González, O., B. Moreno, F. Romanelli and G. F. Panza, 2012. Lithospheric structure below
473 seismic stations in Cuba from the joint inversion of Rayleigh surface waves dispersion and
474 receiver functions, *Geophysical Journal International*, vol. 189, p. 1047-1059.
475

476 Granja-Bruña, J., A. Carbó-Gorosabel, P. L. Estrada, A. Muñoz-Martín, U. ten Brink, M. G.
477 Ballesteros, M. Druet and A. Pazos, 2014. Morphostructure at the junction between the
478 Beata ridge and the Greater Antilles island arc (offshore Hispaniola southern slope),
479 *Tectonophysics*, vol. 618, p. 138-163.
480

481 Gurrola, H., G. E. Baker and J. B. Minster, 1995. Simultaneous time-domain deconvolution
482 with application to the computation of receiver functions, *Geophysical Journal
483 International*, vol. 120, no 3, p. 537-543.
484
485

486 Hammond, J., J.-M. Kendall, G. Stuart, D. Keir, C. Ebinger, A. Ayele and M. Belachew,
487 2011. The nature of the crust beneath the Afar triple junction : Evidence from receiver
488 functions, *Geochemistry, Geophysics, Geosystems*, vol. 12, no 12.

489
490 Hammond, J., J.-M. Kendall, G. Stuart, C. Ebinger, I. Bastow, D. Keir, A. Ayele, M.
491 Belachew, B. Goitom, G. Ogubazghi and collab., 2013. Mantle upwelling and initiation of
492 rift segmentation beneath the Afar Depression, *Geology*, vol. 41, no 6, p. 635-638.

493
494 Hastie, A. R., S. F. Mitchell, P. J. Treloar, A. C. Kerr, I. Neill and D. N. Barfod, 2013.
495 Geochemical components in a Cretaceous island arc : The Th/La-(Ce/Ce*)Nd diagram and
496 implications for subduction initiation in the inter-American region, *Lithos*, vol. 162, p. 57-
497 69.

498
499 Helffrich, G., 2006. Extended-time multitaper frequency domain cross-correlation receiver-
500 function estimation, *Bulletin of the Seismological Society of America*, vol. 96, no 1, p. 344-
501 347.

502
503 Helffrich, G., B. Faria, J. F. Fonseca, A. Lodge and S. Kaneshima, 2010. Transition zone
504 structure under a stationary hot spot: Cape Verde, *Earth and Planetary Science Letters*,
505 vol. 289, no 1, p. 156-161.

506
507 Hernaiz Huerta, P.P., Diaz de Neira, J.A., Garcia Senz, J. Deschamps, I., Genna, A., Nicole,
508 N., Lopera, E., Escuder Virruete, J., Ardevol Oro, Ll., Perez Estaun, A., 2007. La estructura
509 del suroeste de la Republica Dominicana: un ejemplo de deformacion en regimen
510 transpresivo, *Boletin Geologico y Minero*, 118(2) : 337-358.

511
512 Herzberg, C., W. Fyfe and M. Carr, 1983. Density constraints on the formation of the
513 continental Moho and crust, *Contributions to Mineralogy and Petrology*, vol. 84, no 1, p. 1-
514 5.

515
516 Heubeck, C., P. Mann, J. Dolan and S. Monechi, 1991. Diachronous uplift and recycling of
517 sedimentary basins during cenozoic tectonic transpression, northeastern caribbean plate
518 margin, *Sedimentary geology*, vol. 70, no 1, p. 1-32.

519
520 Iturralde-Vinent, M. A., 2006. Meso-Cenozoic Caribbean paleogeography : implications for
521 the historical biogeography of the region, *International Geology Review*, vol. 48, no 9, p.
522 791-827.

523
524 Kamenov, G. D. et al., 2011. Ancient lithospheric source for Quaternary lavas in Hispaniola.
525 *Nature Geoscience*, vol. 4, p. 554-557.

526
527 Kennet, B., 1991. IASPEI 1991 seismological tables, *Terra Nova*, vol. 3, no 2, p. 122-122.

528
529 Langston, C. A., 1979. Structure under Mount Rainier, Washington, inferred from
530 teleseismic body waves, *Journal of Geophysical Research : Solid Earth (1978-2012)*, vol. 84,
531 no B9, p. 4749-4762.

532 Leroy, S., B. Mercier de Lépinay, A. Mauffret and M. Pubellier, 1996. Structural and
533 tectonic evolution of the eastern Cayman Trough (Caribbean Sea) from seismic reflection
534 data, *AAPG bulletin*, vol. 80, no 2, p. 222-247.
535

536 Leroy, S., A. Mauffret, P. Patriat and B. Mercier de Lépinay, 2000. An alternative
537 interpretation of the Cayman trough evolution from a reidentification of magnetic
538 anomalies, *Geophysical Journal International*, vol. 141, no 3, p. 539-557.
539

540 Leroy, S., N. Ellouz-Zimmermann, J. Corbeau, F. Rolandone, B. Mercier de Lépinay, B.
541 Meyer, R. Momplaisir, J. L. Granja Bruna, A. Battani, C. Baurion, E. Burov and collab.,
542 2015. Segmentation and kinematics of the North America-Caribbean plate boundary
543 offshore Hispaniola, *Terra Nova*.
544

545 Ligorria, J. P. and C. J. Ammon, 1999. Iterative deconvolution and receiver-function
546 estimation, *Bulletin of the seismological Society of America*, vol. 89, no 5, p. 1395-1400.
547

548 Lodge, A., S. Nippress, A. Rietbrock, A. García-Yeguas and J. Ibáñez, 2012. Evidence for
549 magmatic underplating and partial melt beneath the canary islands derived using
550 teleseismic receiver functions, *Physics of the Earth and Planetary Interiors*, vol. 212, p. 44-
551 54.
552

553 Mauffret, A. and S. Leroy, 1997. Seismic stratigraphy and structure of the Caribbean
554 igneous province, *Tectonophysics*, vol. 283, no 1, p. 61-104.
555

556 Mauffret, A., Leroy, S., 1999. Neogene intraplate deformation of the Caribbean plate at the
557 Beata Ridge. *Sedimentary Basins of the World 4*, 627-669.
558

559 Mauffret, A., S. Leroy, É. d'Acremont, A. Maillard, B. Mercier de Lépinay, A. T. Dos Reis, N.
560 Miller, A. Nercessian, R. Pérez-Vega and D. Perez, 2001. Une coupe de la province
561 volcanique Caraïbe : premiers résultats de la campagne sismique Casis 2, *Comptes Rendus*
562 *de l'Académie des Sciences-Series IIA-Earth and Planetary Science*, vol. 333, no 10, p. 659-
563 667.
564

565 Mann, P., G. Draper and J. F. Lewis, 1991. An overview of the geologic and tectonic
566 development of Hispaniola, *Geological Society of America Special Papers*, vol. 262, p. 1-28.
567

568 Mann, P. and S. Lawrence, 1991. Petroleum potential of southern Hispaniola, *Journal of*
569 *Petroleum Geology*, vol. 14, no 2, p. 291-308.
570

571 Mann, P., F. Taylor, R. L. Edwards and T.-L. Ku, 1995. Actively evolving microplate
572 formation by oblique collision and sideways motion along strike-slip faults : An example
573 from the northeastern Caribbean plate margin, *Tectonophysics*, vol. 246, no 1, p. 1-69.
574

575 Martinez-Arevalo, C., F. de Lis Mancilla, G. Helffrich and A. Garcia, 2013. Seismic evidence
576 of a regional sublithospheric low velocity layer beneath the Canary islands, *Tectonophysics*,

577 vol. 608, p. 586-599.

578

579

580 McNamara, D., M. Meremonte, J. Maharrey, S.-L. Mildore, J. Altidore, D. Anglade, S.
581 Hough, D. Given, H. Benz, L. Gee and collab., 2012. Frequency-dependent seismic
582 attenuation within the Hispaniola Island region of the Caribbean Sea, *Bulletin of the*
583 *Seismological Society of America*, vol. 102, no 2, p. 773-782.

584

585 Meschede, M. and W. Frisch, 1998. A plate-tectonic model for the Mesozoic and Early
586 Cenozoic history of the Caribbean plate, *Tectonophysics*, vol. 296, no 3, p. 269-291.

587

588 Moreno, B., M. Grandison and K. Atakan, 2002. Crustal velocity model along the southern
589 Cuban margin : implications for the tectonic regime at an active plate boundary,
590 *Geophysical Journal International*, vol. 151, no 2, p. 632-645.

591

592 Nuñez, D., D. Cordoba, F. J. Nuñez-Cornu and M. O. Cotilla, 2015. Lithosphere structure
593 from Cordillera Central to Cordillera Oriental (Dominican Republic), *EGU General Assembly*
594 *Conference Abstracts*, vol. 17, p. 14467.

595

596 Owens, T., S. Taylor and G. Zandt, 1983. Isolation and enhancement of the response of
597 local seismic structure from teleseismic P-waveforms, *cahier de recherche*, Lawrence
598 Livermore National Lab., CA (USA).

599

600 Park, J. and V. Levin, 2000. Receiver functions from multiple-taper spectral correlation
601 estimates, *Bulletin of the Seismological Society of America*, vol. 90, no 6, p. 1507-1520.

602

603 Pindell, J., L. Kennan, K. P. Stanek, W. Maresch and G. Draper, 2006. Foundations of Gulf
604 of Mexico and Caribbean evolution: eight controversies resolved, *Geologica Acta*, vol. 4, no
605 1-2, p. 303.

606

607 Pindell, J., W. V. Maresch, U. Martens and K. Stanek, 2012. The Greater Antillean Arc :
608 Early Cretaceous origin and proposed relationship to Central American subduction mélanges
609 : implications for models of Caribbean evolution, *International Geology Review*, vol. 54, no
610 2, p. 131-143.

611

612 Pubellier, M., A. Mauffret, S. Leroy, J. M. Vila and H. Amilcar. 2000, «Plate boundary
613 readjustment in oblique convergence : Example of the Neogene of Hispaniola, Greater
614 Antilles», *Tectonics*, vol. 19, no 4, p. 630-648.

615

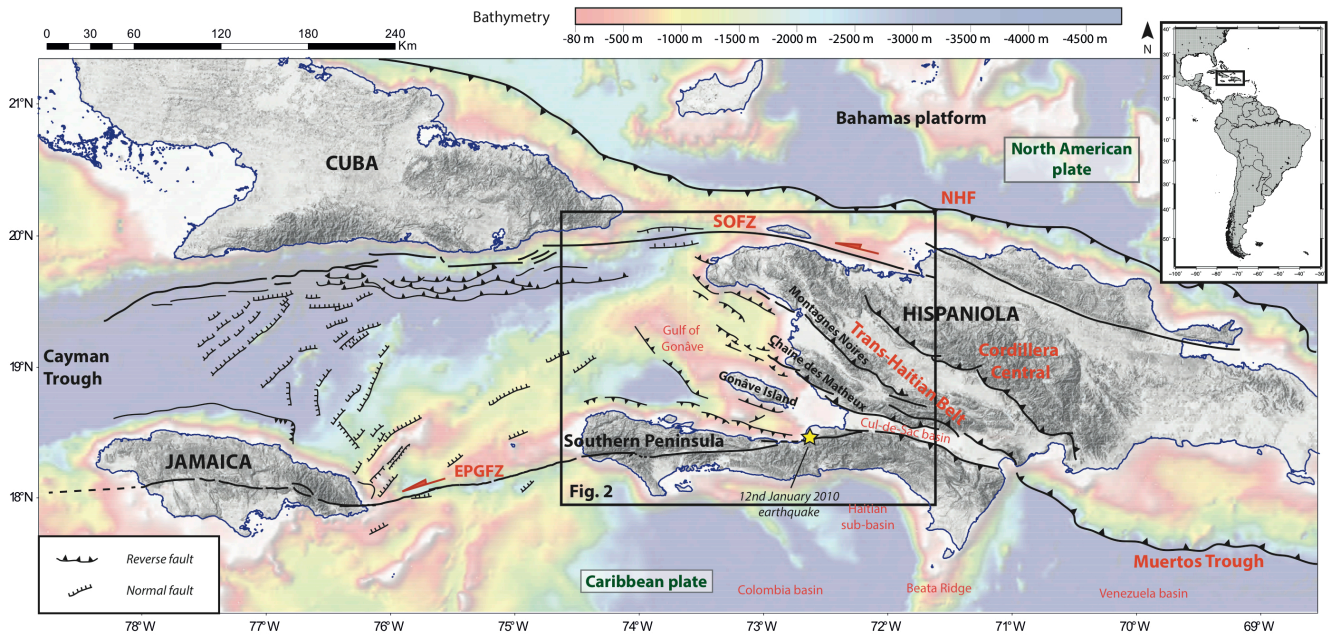
616 Revillon, S., E. Hallot, N. Arndt, C. Chauvel and R. Duncan, 2000. A complex history for the
617 Caribbean Plateau: petrology, geochemistry, and geochronology of the Beata Ridge, South
618 Hispaniola, *The Journal of Geology*, vol. 108, no 6, p. 641-661.

619

620 Rossi, G., Abers, G. A., Rondenay, S., & Christensen, D. H., 2006. Unusual mantle Poisson's
621 ratio, subduction, and crustal structure in central Alaska, *Journal of Geophysical Research:*
622 *Solid Earth*, vol. 111, no B9.

623
624
625
626 Saint Fleur, N., N. Feuillet, R. Grandin, E. Jacques, J. Weil-Accardo and Y. Klinger, 2015.
627 Seismotectonics of southern Haiti: A new faulting model for the 12 January 2010 M7
628 earthquake, *Geophysical Research Letters*.
629
630 Symithe, S. and E. Calais, 2016. Present-day shortening in Southern Haiti from GPS
631 measurements and implications for seismic hazard, *Tectonophysics*, 679, 117-124.
632
633 Symithe, S., E. Calais, J. B. Chabalier, R. Robertson and M. Higgins, 2015. Current block
634 motions and strain accumulation on active faults in the Caribbean, *Journal of Geophysical*
635 *Research: Solid Earth*, 120(5), 3748-3774.
636
637 Stéphan, J.-F., B. Mercier de Lépinay, E. Calais and M. Tardy, 1990. Paleogeodynamic maps
638 of the Caribbean: 14 steps from Lias to Present, *Bull. Soc. géol. Ft*, p. 0-6.
639
640 Stuart, G., I. Bastow and C. Ebinger, 2006. Crustal structure of the northern Main Ethiopian
641 Rift from receiver function studies, *Geological Society*, London, Special Publications, vol.
642 259, no 1, p. 253-267.
643
644 Thompson, D., I. Bastow, G. Helffrich, J. Kendall, J. Wookey, D. Snyder, and D. Eaton,
645 2010. Precambrian crustal evolution: Seismic constraints from the Canadian Shield, *Earth*
646 *Planet. Sci. Lett.*, 297, 655-666, doi:10.1016/j.epsl.2010.07.021.
647
648 Thurber, C., S. Roecker, K. Roberts, M. Gold, L. Powell and K. Rittger, 2003. Earthquake
649 locations and three-dimensional fault zone structure along the creeping section of the San
650 Andreas fault near Parkfield, CA : Preparing for SAFOD, *Geophysical Research Letters*, vol.
651 30, no 3.
652
653 VanDerLelij, R., 2013. Reconstructing north-western Gondwana with implications for the
654 evolution of the Iapetus and Rheic Oceans: a geochronological, thermochronological and
655 geochemical study, thèse de doctorat, University of Geneva.
656
657 Watanabe, T., 1993. Effects of water and melt on seismic velocities and their application to
658 characterization of seismic reflectors, *Geophysical Research Letters*, vol. 20, no 24, p.
659 2933-2936.
660
661 Witschard, M. and J. F. Dolan, 1990. Contrasting structural styles in siliciclastic and
662 carbonate rocks of an offscraped sequence: The Peralta accretionary prism, Hispaniola,
663 *Geological Society of America Bulletin*, vol. 102, no 6, p. 792-806.
664
665 Zandt, G. and C. J. Ammon, 1995. Continental crust composition constrained by
666 measurements of crustal Poisson's ratio, *Nature*, vol. 374, no 6518, p. 152-154.
667

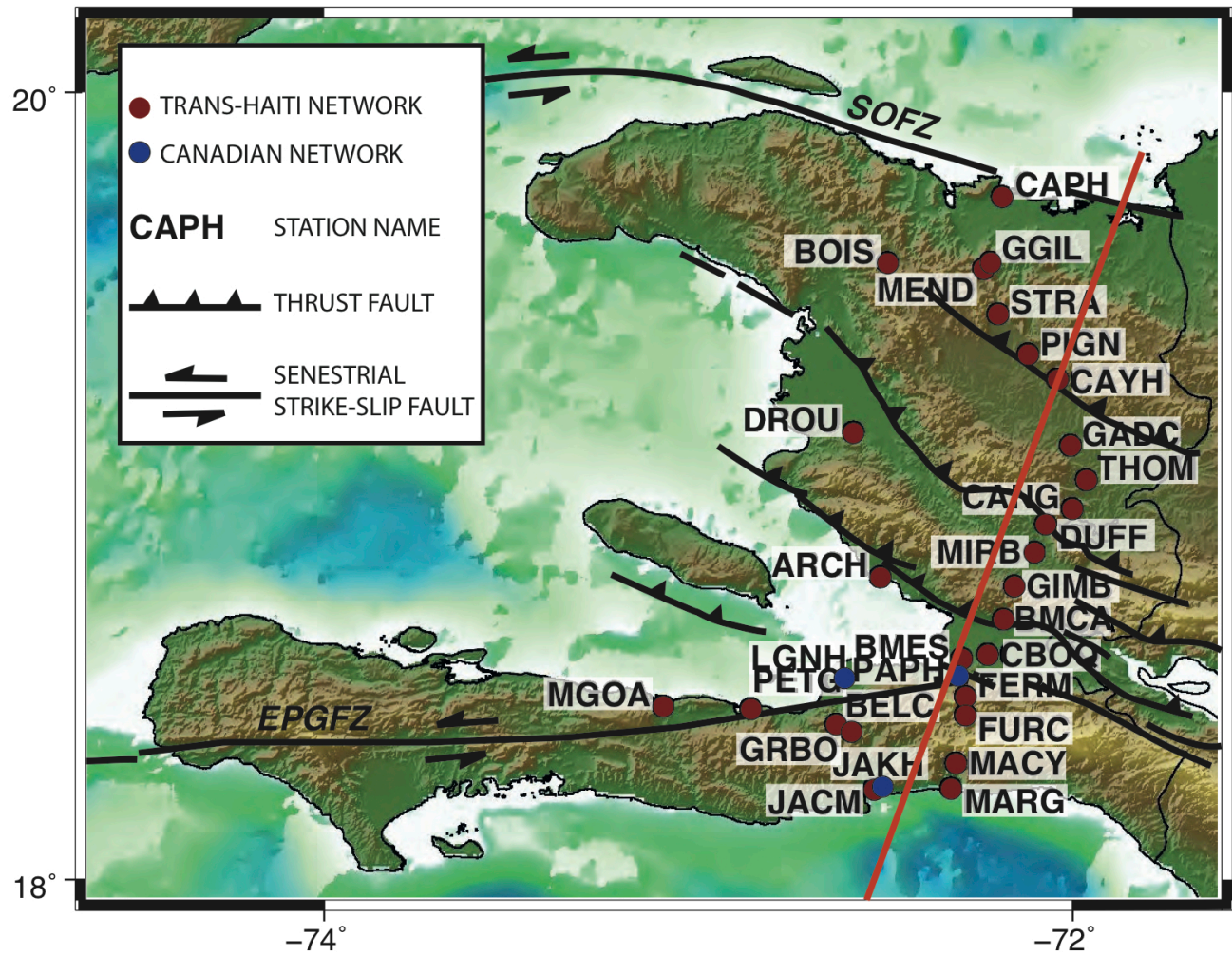
668 Zhao, D., H. Kanamori, H. Negishi and D. Wiens, 1996. Tomography of the source area of
669 the 1995 kobe earthquake : evidence for fluids at the hypocenter ?, *Science*, vol. 274, no
670 5294, p. 1891-1894.
671 Zhu, L. and H. Kanamori, 2000. Moho depth variation in southern California from
672 teleseismic receiver functions, *Journal of Geophysical Research B*, vol. 105, no B2, p. 2969-
673 2980.



674

675 **Figure 1:** Tectonic map of the Northern Caribbean plate boundary. Faults are from previous
 676 studies (Calais and Mercier de Lépinay, 1991; Mann et al., 1995; Leroy et al., 1996; 2015;
 677 Granja Bruna et al., 2014). NHF: North-Hispaniola Fault; SOFZ: Septentrional-Oriente Fault
 678 Zone; EPGFZ: Enriquillo-Plantain-Garden Fault Zone.

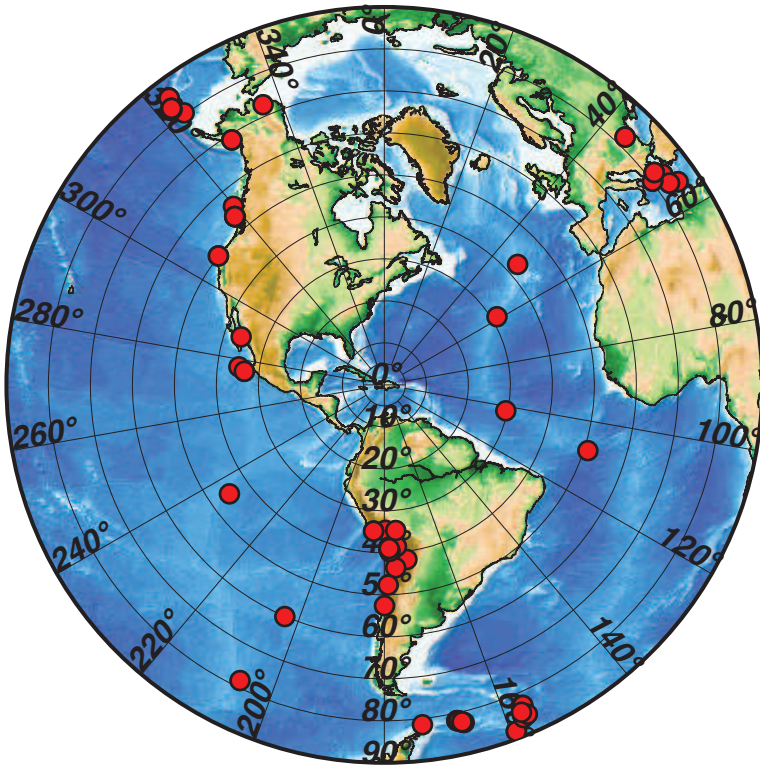
679



680

681 **Figure 2:** Locations of the seismic stations used in this receiver function study in Haiti,
 682 superimposed on the topographic map and with the major tectonic features. Red circles are
 683 the stations of the Trans-Haiti network and blue circles are the 3 permanent stations of the
 684 Canadian National Network. Faults are from Pubellier et al. (2000). SOFZ: Septentrional-
 685 Oriente Fault Zone; EPGFZ: Enriquillo-Plantain-Garden Fault Zone. The red line indicates
 686 the localization of the transect proposed Fig. 10.

687



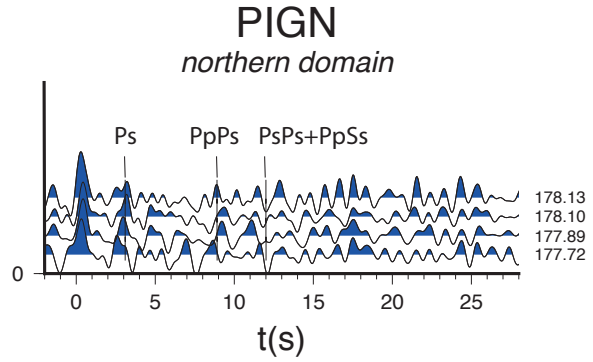
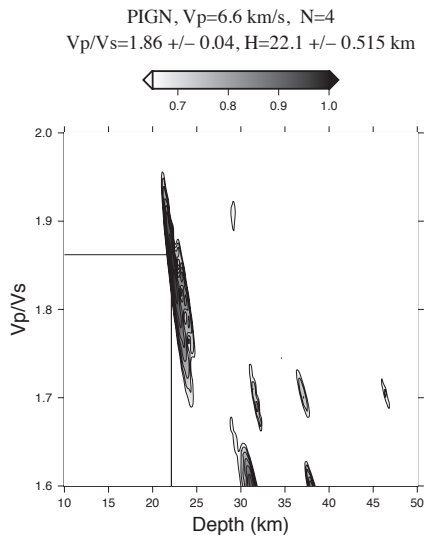
688

689 **Figure 3:** Global distribution of the earthquakes used when computing Receiver Functions.

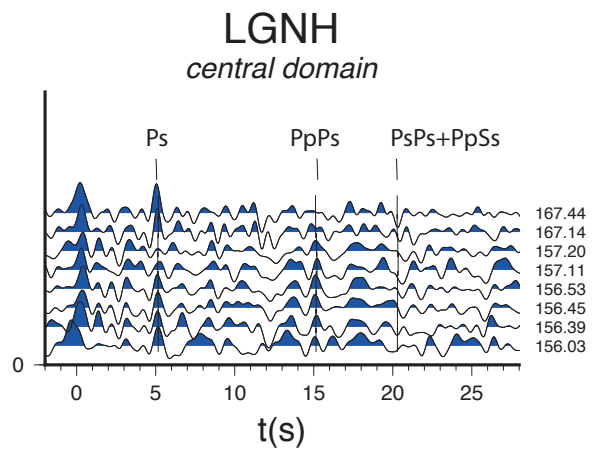
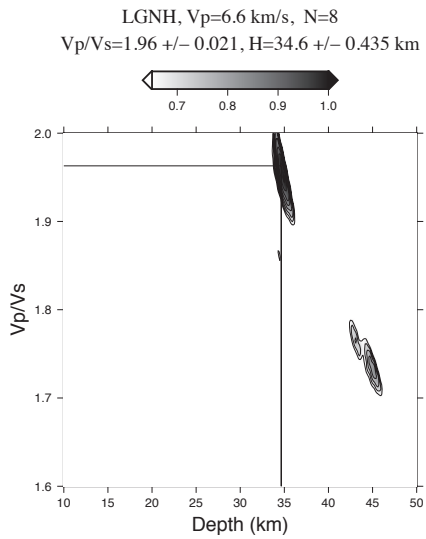
690 They are plotted with an azimuthal equidistant map projection around our network.

691

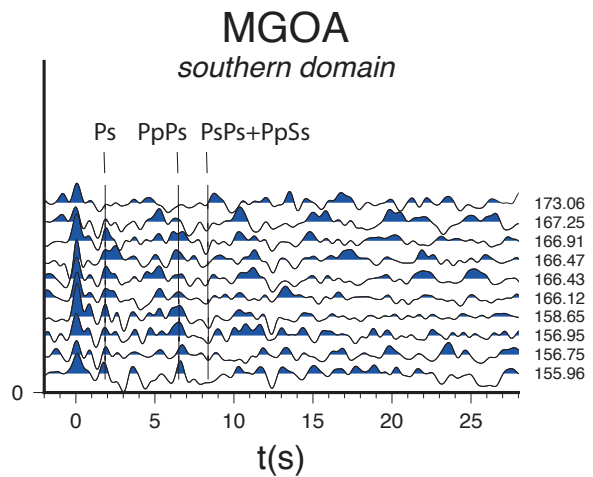
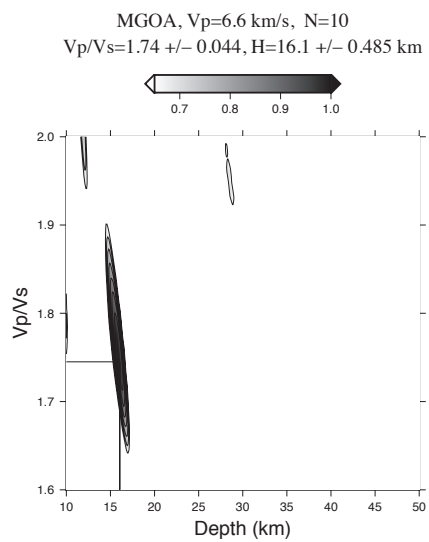
i.



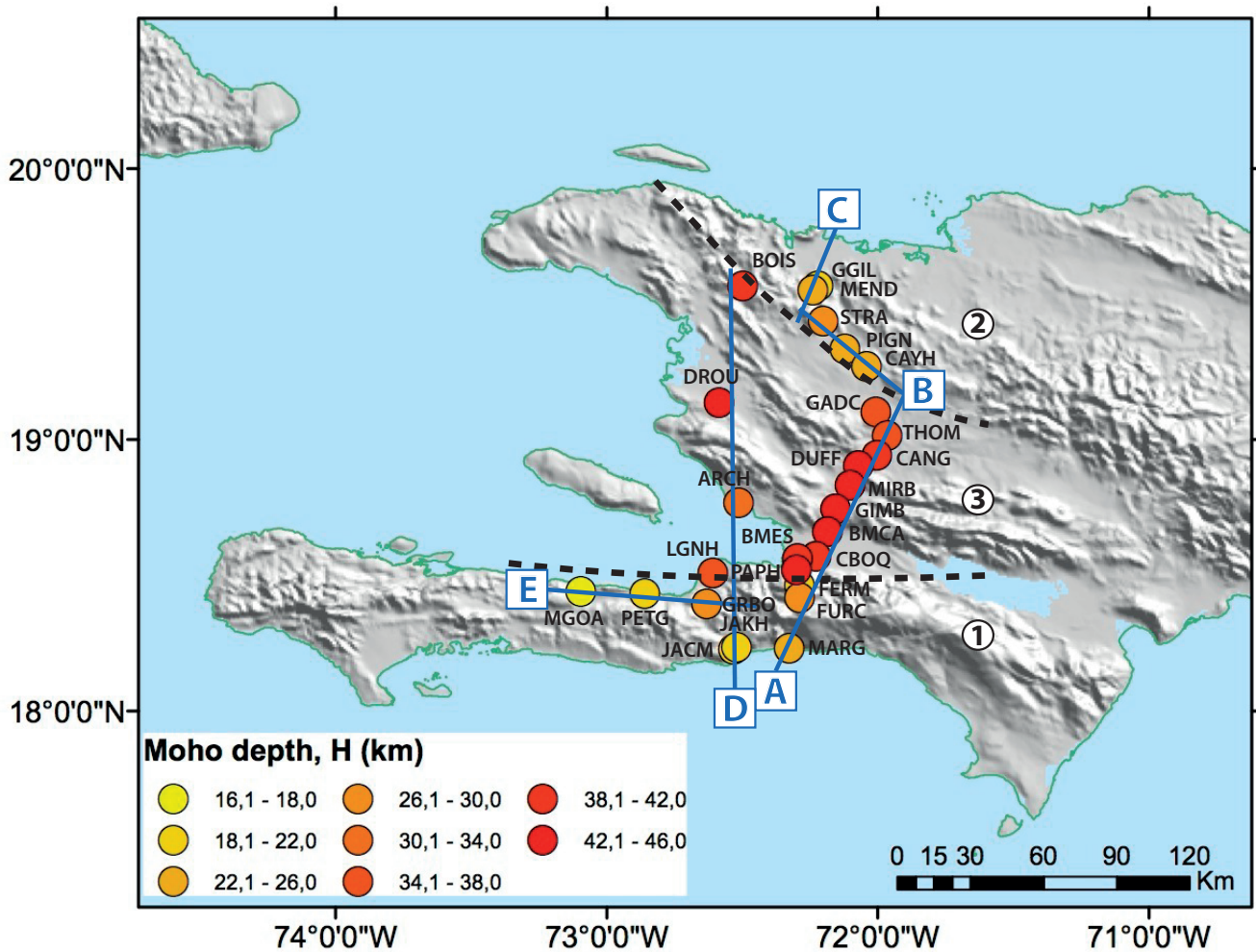
ii.



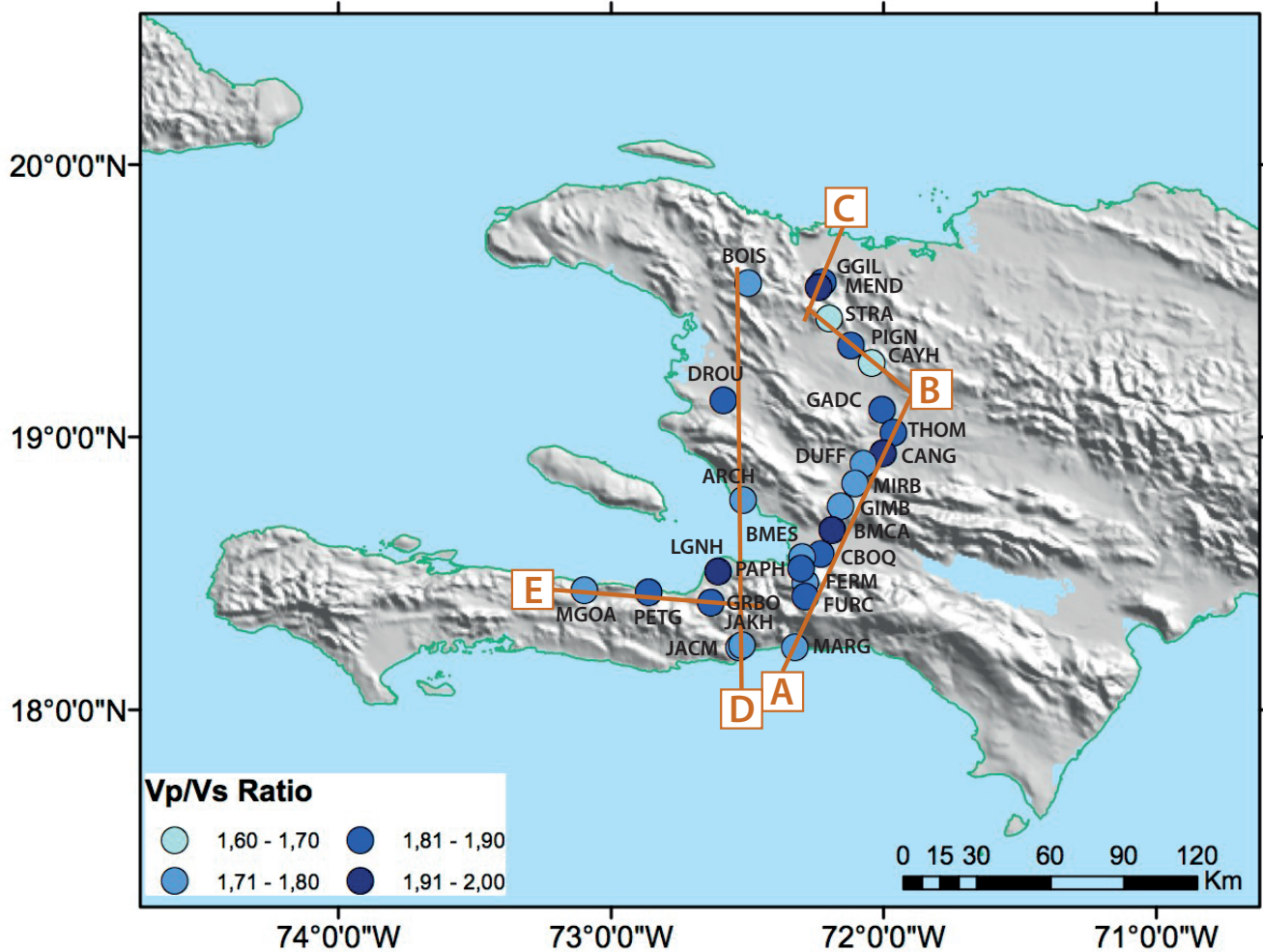
iii.



693 **Figure 4:** Examples of Moho depth (H) versus Vp/Vs plots (left) from the method of Zhu and
 694 Kanamori (2000) and receiver functions associated (right) for one station of each domain.
 695 On each receiver function the arrival time of the Moho phase Ps (t1) and the reverberations
 696 PpPs (t2) and PsPs+PpSs (t3) are marked based on the results of the H-K stack (Table 1) and
 697 the equations (2) to (4). The receiver functions are plotted as a function of the back-
 698 azimuth (number at the right of each trace). See Figs. 2 and 5 for the location of the
 699 stations and the different domains.
 700



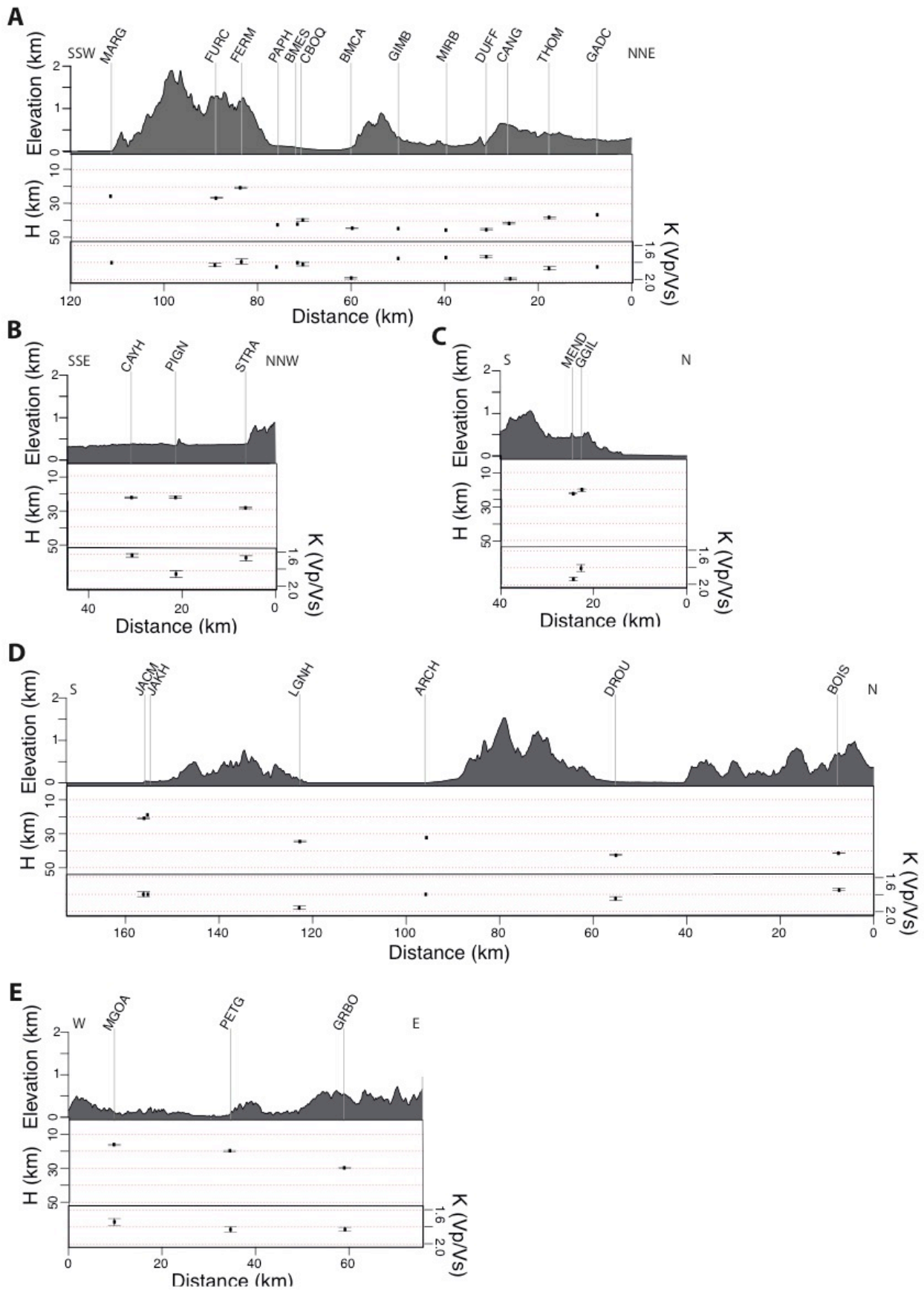
701
 702 **Figure 5:** Variations in Moho depth (Tables 1 and 2) across Haiti determined from receiver
 703 function analysis. The blue lines A, B, C, D, and E show the orientation of transects in
 704 Figure 7. The black dashed lines delimit the boundary between 3 distinct domains of Moho
 705 depth values, numbered 1, 2 and 3 (see text for explanation).



706

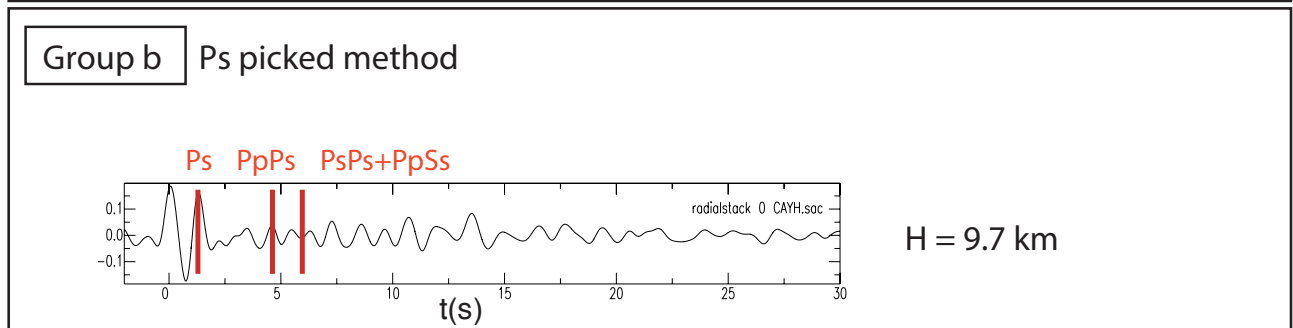
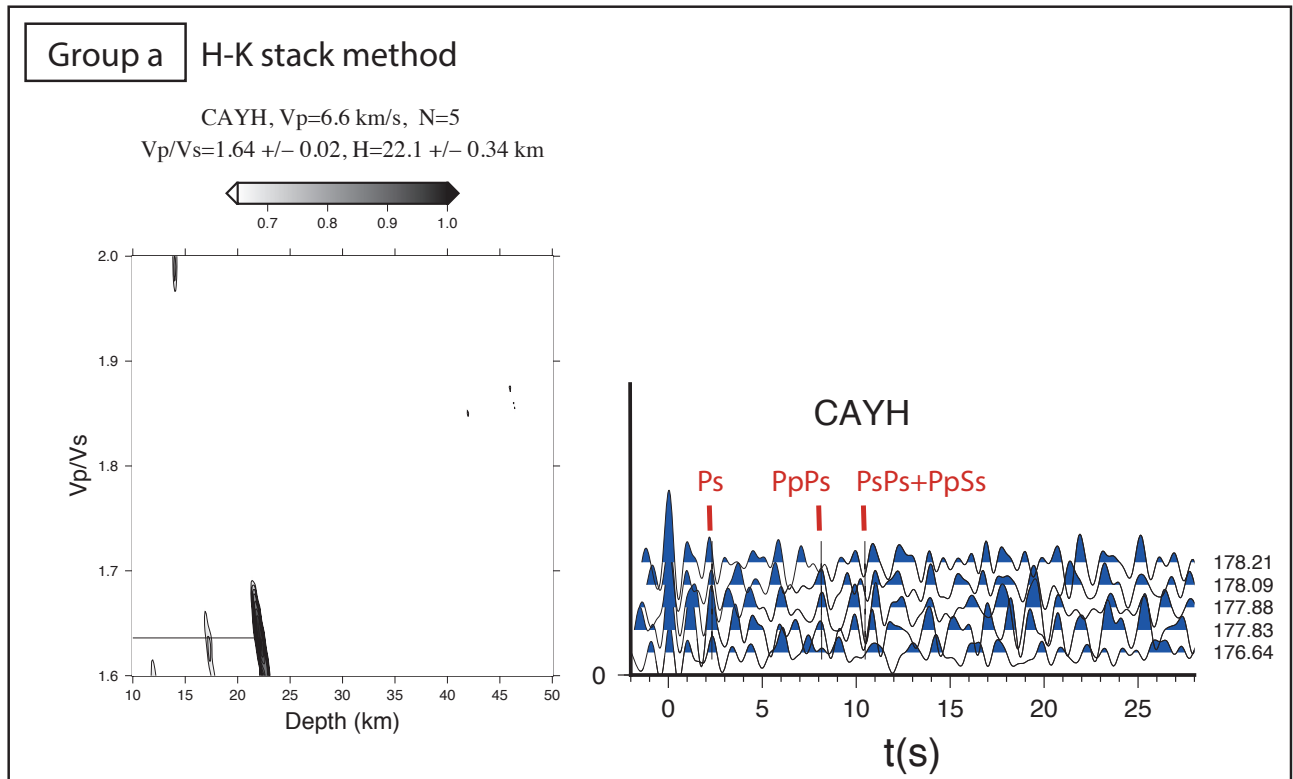
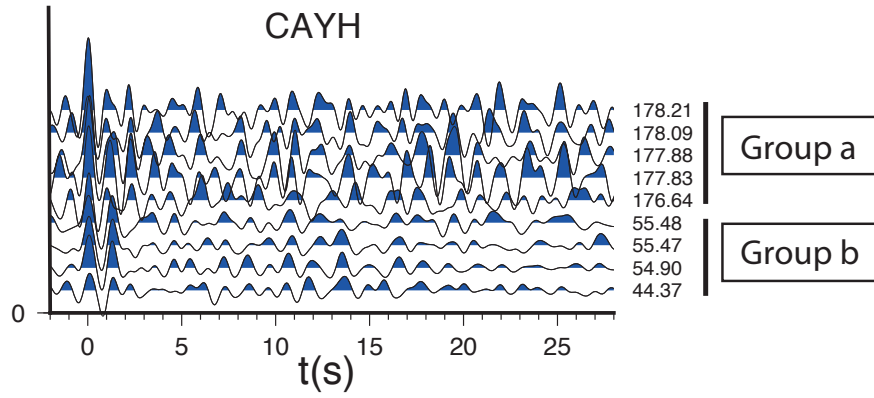
707 **Figure 6:** Variations in V_p/V_s ratio (Tables 1 and 2) across Haiti determined from receiver
 708 function analysis. The orange lines A, B, C, D, and E show the orientation of transects in
 709 Figure 7.

710



712 **Figure 7:** Variations in elevation, Moho depth, and V_p/V_s ratio across Haiti. The elevation
713 exaggeration is x10. (A) SW-NW across the central and southern part of Haiti, (B) and (C)
714 SE-NW and SW-NE across the northern part of Haiti, (D) S-N across the West of the central
715 and southern part, and (E) W-E across the southern part of Haiti. The orientations of the
716 transects are shown on Figures 5 and 6.

717

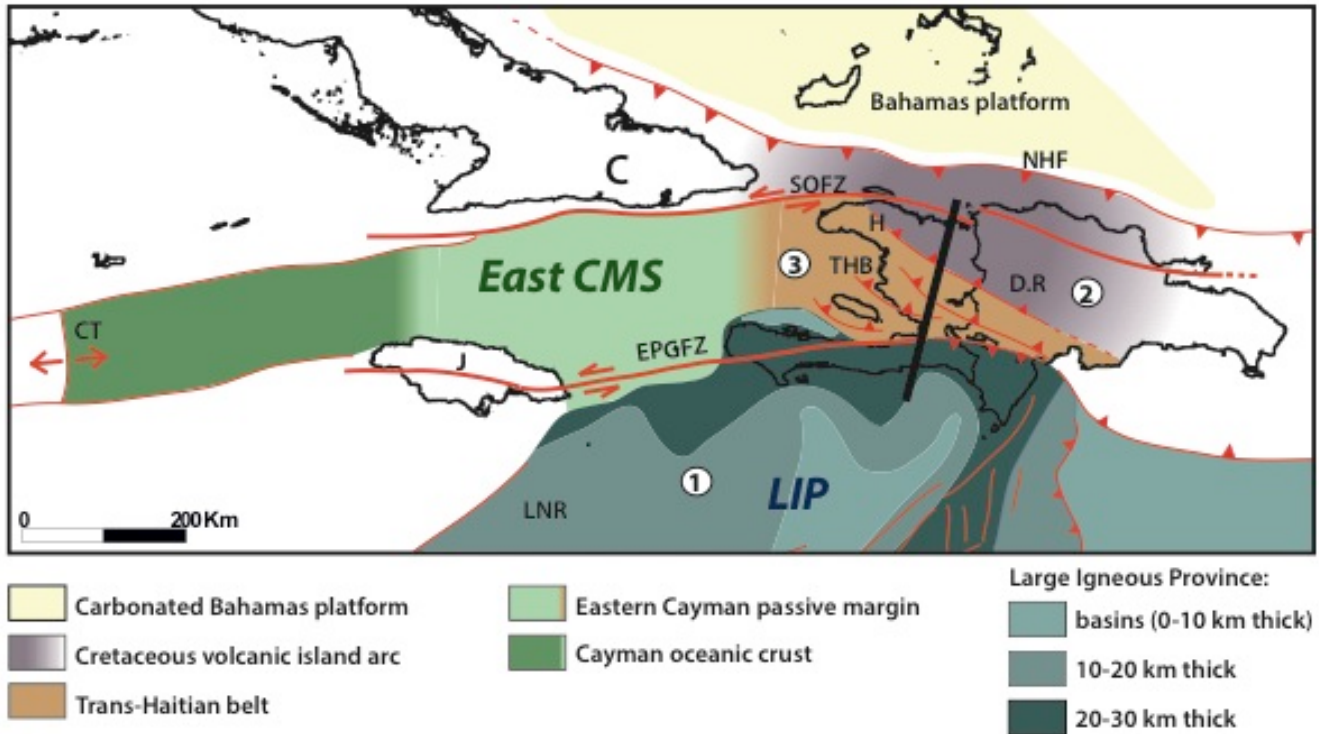


718

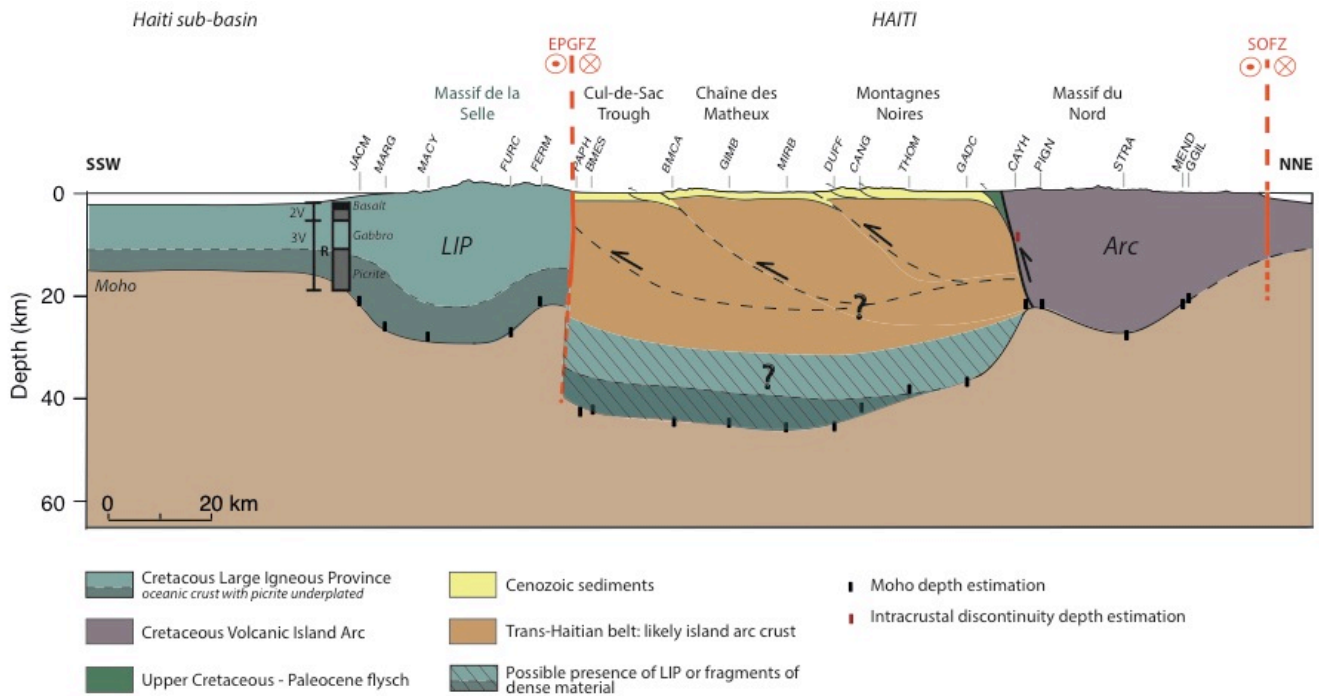
719

720

721 **Figure 8:** Estimation of the depth of an intracrustal layer for the station CAYH. The Moho
 722 depth is estimated at 22.1 km with Ps arrival and PpPs and PsPs+PpSs reverberations, using
 723 the H-K stack method and the RFs coming from the South (back-azimuth of about 170°,
 724 group a). A reverberation is imaged before the Ps arrival on RFs coming from the North-East
 725 (back-azimuth of about 55°, group b), and the corresponding estimated depth with Ps
 726 picked method ($V_p=5.8$ km/s and $K=1.77$) is 9.7 km.
 727



728
 729 **Figure 9:** Location of the proposed different crustal domains we identified in Hispaniola.
 730 (1) the Caribbean Large Igneous Province, (2) the Cretaceous island arc and (3) the fold and
 731 thrust belt. C: Cuba; J: Jamaica; H: Haiti; D.R: Dominican Republic. NHF: North Haitian
 732 Fault; SOFZ: Septentrional-Oriente Fault Zone; THB: Trans-Haitian Belt; EPGFZ: Enriquillo-
 733 Plantain-Garden Fault Zone; CT: Cayman Trough; LNR: Lower Nicaraguan Rise. East CMS:
 734 eastern Cayman Trough margin system; LIP: Large Igneous Province. The black line
 735 indicates the localization of the transect shown in Fig. 10. The thicknesses of the LIP at
 736 sea are from Mauffret and Leroy (1997). The boundary between the East CMS and the LIP at
 737 sea is from Corbeau et al. (2016a).
 738



739

740 **Figure 10:** Summary conceptual geological transect across Haiti based on the Moho and
 741 intracrustal discontinuity depths. See Figs 2 and 9 for location of the profile. The
 742 seismologic stations are indicated. EPGFZ: Enriquillo-Plantain-Garden fault zone; SOFZ:
 743 Septentrional-Oriente fault zone. The log south of the transect is a model of the LIP crustal
 744 thickness based on a compilation of seismic refraction results: the layer 2V (original oceanic
 745 crust) is sandwiched between an upper basaltic layer (in black) and the layer 3V (original
 746 crust underplated); R is the top of a high velocity layer (Mauffret and Leroy, 1997).

Table 1: Moho depth (H) and Vp/Vs ratio (κ) estimated by the H-K stacking method

Stations	N	H(km)	δH (km)	K	δK
BMCA (line A)	13	44.3	0.1	1.98	0.01
BOIS (line D)	2	41.5	0.1	1.75	0.01
CANG (line A)	4	41.5	0.4	1.99	0.01
CAYH (line B)	5	22.1	0.4	1.64	0.02
CBOQ (line A)	7	39.5	0.7	1.82	0.02
DROU (line D)	7	47.2	0.4	1.85	0.02
DUFF (line A)	3	45.2	0.4	1.73	0.01
FERM (line A)	2	20.5	0.4	1.79	0.03
FURC (line A)	3	26.6	0.3	1.83	0.02
GGIL (line C)	3	20.1	0.7	1.81	0.04
GRBO (line E)	3	29.8	0.3	1.83	0.02
JACM (line D)	3	20.9	0.4	1.80	0.03
LGNH (line D)	8	34.6	0.4	1.96	0.02
MEND (line C)	6	22.5	0.4	1.94	0.02
MGOA (line E)	10	16.1	0.5	1.74	0.04
PETG (line E)	3	19.7	0.4	1.83	0.03
PIGN (line B)	4	22.1	0.5	1.86	0.04
STRA (line B)	4	28.2	0.4	1.67	0.03
THOM (line A)	5	37.9	0.5	1.87	0.02

1 **Table 2: Moho depth (H) estimated by Ps picked method**

Stations	N	H(km)	K
ARCH (line D)	5	32.3	1.80
BMES (line A)	5	41.9	1.80
GADC (line A)	4	36.4	1.85
GIMB (line A)	9	44.5	1.75
JAKH (line D)	9	19.0	1.80
MARG (line A)	3	25.5	1.80
MIRB (line A)	3	45.4	1.74
PAPH (line A)	9	42.3	1.85

2